2018 22nd International Conference on System Theory, Control and Computing (ICSTCC)

Gradient-free navigation of a nonholonomic robot for tracking unsteady environmental boundaries in 3D

Alexey S. Matveev
Department of Mathematics and Mechanics
Saint Petersburg State University
28 Universitetsky Pr., St. Petersburg, 198504, Russia
Faculty of Control Systems and Robotics
ITMO University
49 Kronverksky Pr., St. Petersburg, 197101, Russia
almat1712@yahoo.com

Anna A. Semakova
Department of Mathematics and Mechanics
Saint Petersburg State University
28 Universitetsky Pr., St. Petersburg, 198504, Russia
Russian State Scientific Center for Robotics
and Technical Cybernetics
21 Tikhoretsky Pr., St. Petersburg, 194064, Russia
a.semakova@gmail.com

***Abstract*—An underactuated nonholonomic robot with a bounded control input travels with a constant speed in a 3D workspace. An unknown time variant scalar field is defined on this workspace. The robot should detect, locate, and densely sweep a moving and deforming 2D isosurface (level set), which is the locus of points where the field takes a given value. The sensory data consist of the value of the field at the current location, robot's coordinate along a certain (typically, vertical) space direction, and the orientation of this direction relative to the robot. We offer a new navigation law under which the robot reaches the targeted isosurface from an occasional initial location and then scans the part of this surface in between two given "altitudes". This law does not rely on estimation of the field gradient and is undemanding in terms of motion and computation. Its convergence is demonstrated by a mathematically rigorous result and computer simulation tests.**

***Index Terms*—Mobile robots, sensor based 3D navigation, tracking environmental level sets**

I. INTRODUCTION

Robotic tracking and monitoring of environmental boundaries has received considerable attention over the last two decades due to an ever-expanding range of applications. Examples include detection of and surveillance over contaminant clouds [1] or areas of harmful algal blooms [2], to name just a few. Typically, the mission is to locate and reach the set where an environmental field assumes a certain value and to subsequently move over this level set, with the intention to repeatedly cover it via a sort of a "sweeping" maneuver. As a result, the robot exposes and takes control over the border of the region where the field takes greater values, which region is often the true focus of interest. In such missions, the field value can be often measured only at the robot's current location.

Existing methods of robotic tracking of environmental boundaries can be categorized into gradient based and gradient free approaches. The former rely on knowledge of the field gradient. Examples include methods descended from the snake algorithms for contour detection [3], [4], gradient based contour evaluation [3]–[5] or implementation of the artificial potentials approach [6], cooperative estimation of the gradient by a group of mobile robots [7], etc. However, it is not rare that the field derivatives are not directly measured. Meanwhile, their evaluation on the basis of the field value measurements requires to perform them at several nearby locations and to gather these data at a common decision center. Even for scenarios with many sensors, the former may call for their unproductive clustering, whereas the latter may be impeded by communication limitations.

Gradient free methods are mostly concerned with a single field sensor and do not noticeably attempt at estimation of the field gradient. In [8], [9], threshold-triggered switching between two steering angles is advocated; a similar rule with many angles is proposed in [10] for an underwater vehicle. Such rules ordinarily entail oscillating around the principal, i.e., averaged, path, thus actually using systematic and mutually nullifying shifts sideways to accumulate field data from a whole corridor. In [11], tracking a fire-front by an aerial vehicle is underlaid by segmentation of the forest fire images. These control laws are more or less based on heuristics and were not substantiated by rigorous and completed justification. In [12], the suggested PD controller is justified by rigorously showing its local convergence in radial harmonic fields for a Dubins-car robot with an infinite control range. Gradient-free sliding mode controllers were offered in [13] and [14] in the cases of steady and dynamic fields, respectively, and a Dubins-car vehicle with a finite control range; they were substantiated by rigorous global convergence results in generic smooth fields.

The ever expanding use of autonomous underwater, aerial, and space vehicles stimulates the interest in robots that face the need to move in all three dimensions. Many missions on tracking of natural boundaries are carried out in 3D workspaces so

---

This work was supported by the Russian Science Foundation (RSF, Proj. No 14-21-00041p).

978-1-5386-4444-7/18/$31.00 ©2018 IEEE

that the robot should regard all three dimensions as feasible options of motion direction. However, the authors failed to come across a paper on robotic tracking of environmental level sets that addresses 3D workspaces. The present paper aims to fill in this gap, with a focus on nonholonomic, under-actuated robots with a priori limited control range.

To this end, we use the standard extension of the Dubins car model to the case of 3D [15], [16]: a robot moves in 3D in the surge direction, the speed is constant, the control inputs are the yawing and pitching rates. They are bounded; so the robot's turning radius is lower limited. As is discussed in [15], [16], this model is applicable to missiles, torpedo-like UUV's, fixed-wing UAV's, and in the cases where the acceleration vector is manipulable within a disk perpendicular to the velocity, like for many rotary-wing aircraft. There is coupling between the vertical and horizontal control loops: the "vertical" control has direct impact on the "horizontal" motion since the only way to affect the motion in the vertical direction is to alter the angle between the constant-magnitude velocity and the horizontal.

The considered time-varying scalar fields in 3D are arbitrary, up to a few technical assumptions that are inevitable in some ways. The robot has access to the value assumed by the field at the robot's position. The robot is also able to evaluate the rate of change of this reading in time, e.g., by means of numerical differentiation. The sensors supply information about the robot's coordinate along a certain space direction and the orientation of this direction relative to the robot.

To sweep the isosurface, we implement spiralling over it, with drifting in the above direction. Such pattern makes arbitrarily dense coverage possible (at least for steady fields) if only the inevitable condition is met: the robot's turning radius is enough to handle the contortions of the isosurface.

We propose a navigation law that employs neither gradient estimation nor systematic sideway exploratory maneuvers. It is thrifty not only with motion but also with computational resources: the current observation is directly transformed into the control input via a few arithmetic operations. We start with disclosing conditions necessary in order that the considered robot can perform sweep coverage of the time-varying isosurface of interest. Then it is rigorously shown that under minor and, in some ways, inevitable enhancement of these conditions, the proposed navigation law proves itself to be sufficient to solve the mission and to ensure global convergence, despite many limitations such as nonholonomy, underactuation, finite control range, sensorial deficiency, etc. This holds provided that the controller is properly tuned; respective recommendations are explicitly presented. Basic theoretically grounded findings are underpinned by simulation experiments.

This paper extends some ideas given in [13], [14], [17]–[20]. In particular, the model of the robot's three dimensional kinematics is taken from [18]. Meanwhile, only two dimensional workspaces were treated in the other papers, and so their accomplishments are not sufficient to cope with some special challenges caused by 3D environments. With an intention only to illustrate this rather than to delve into full details, we note that the findings of these papers are not directly applicable even to the 2D projection of the robot since contrary to their assumptions, this projection does not obey the Dubins car model. Also those papers give no recipe to resolve intricacies stemming from coupling between the "vertical" and "horizontal" control loops.

Organization of the paper. Section II describes the studied system and gives the statement of the problem, Section III presents the navigation law. Section IV discusses necessary conditions and theoretical assumptions. Sections V and VI deal with the closed-loop system and offer the results of theoretical analysis and computer simulations, respectively. Due to the page limit, the proofs of the presented theoretical results will be given in the full version of the paper.

Throughout the paper, we use the following notations:

- $\|\cdot\|$, $\langle \cdot ; \cdot \rangle$, and $\times$, standard Euclidean norm, inner product, and cross product in $\mathbb{R}^3$, respectively;
- $\boldsymbol{r} \in \mathbb{R}^3$, location of the robot;
- $D(\boldsymbol{r}, t)$, unsteady environmental field in the space $\mathbb{R}^3$;
- $d(t) = D[\boldsymbol{r}(t), t]$, its value at the location of the robot;
- d_0, targeted field value;
- $S_t(d_0) = \{\boldsymbol{r} : D(\boldsymbol{r}, t) = d_0\}$, time-varying locus of points with the field value d_0 called *isosurface*;
- v, robot's speed;
- $\boldsymbol{u}$ and $\overline{u}$, acceleration vector of the robot and the upper bound on the magnitude of this vector;
- $\boldsymbol{\imath}$, unit vector in the surge direction;
- $\boldsymbol{h}$, unit vector in the "vertical" direction;
- h, "vertical" coordinate of the robot;
- $[h_-, h_+]$, interval of robot's operational "altitudes";
- $\boldsymbol{\imath}_h$, vector $\boldsymbol{h}$ projected onto the plane normal to $\boldsymbol{\imath}$ and then scaled to the unit length;
- d_-, d_+, respectively, minimum and maximum values of the field in the operational zone $\mathcal{M}$ of the robot;
- $\sphericalangle(\vec{a}, \vec{b})$, angle between the nonzero vectors $\vec{a}, \vec{b} \in \mathbb{R}^3$.

II. SYSTEM DESCRIPTION AND PROBLEM SETUP

In a three-dimensional workspace, a robot moves in the surge direction with a constant speed v; the pitch and yaw rates are the control inputs. They are upper limited and so the robot's turning radius is lower bounded. A scalar field is defined on the workspace; this field varies over time and maps any point $\boldsymbol{r} \in \mathbb{R}^3$ into $D(\boldsymbol{r}, t) \in \mathbb{R}$ at time t. Starting from an occasional location, the robot should arrive at the moving and deforming isosurface $S_t(d_0)$, which is the locus of points in space where the field takes a pre-specified value d_0. Afterwards, the robot should not only remain on this isosurface but also densely sweep it. The robot does not know the field in advance and can measure only the field value $d(t) := D(\boldsymbol{r}, t)$ at the current location $\boldsymbol{r} = \boldsymbol{r}(t)$. Neither the field gradient, nor its parts, nor the time derivative D_t' are accessible.

Not the entire surface $S_t(d_0)$ is to be swept. The zone of interest is defined by means of a certain unit vector $\boldsymbol{h} \in \mathbb{R}^3$ and the coordinate h along $\boldsymbol{h}$. They are called the *vertical* vector and *altitude*, respectively, although these names literally conform only to a particular howbeit fairly common scenario.

The duty of the robot does not extend outside a given interval of altitudes $[h_-, h_+], h_- < h_+$, which may be based on e.g., allocation of duties among many robots, operational altitude range of the robot, or priorities among altitudes.

If $S_t(d_0)$ expands from h_- to h_+, sweeping the targeted part $S_t^e(d_0) := \{\boldsymbol{r} \in S_t(d_0) : h \in [h_-, h_+]\}$ of $S_t(d_0)$ involves reaching $h_\pm$, after which $h \in [h_-, h_+]$ cannot be retained due to the inertia, unless the velocity is horizontal. So among many patterns of dense sweep coverage of S_t^e, densely coiling on S_t^e with nearly horizontal loops looks like a good option since then the velocity direction is automatically close to horizontal. Another attractive feature is that no demands to the turning capacity of the robot are imposed by this pattern itself, unlike, e.g., the popular lawn-mowing survey. The small vertical step between the coils should be reversed near the extreme altitudes to respect the range $[h_-, h_+]$. If the examined part $S_t^e(d_0)$ of the isosurface has several connected components, only one of them should be covered.

The sensors measure the orientation of $\boldsymbol{h}$ relative to the robot's body and the altitude $h(\boldsymbol{r})$ of the robot.

Defintion 1: The robot is said to *perform coiling sweep coverage of the isosurface* within the interval $[h_-, h_+]$ of altitudes and with the vertical speed $v_h \in (0, v)$ if $d(t) \to d_0$ as $t \to \infty$ and there is a partition of $[0, \infty)$ into uniformly bounded intervals $0 < \tau_0^- < \tau_0^+ < \tau_1^- < \tau_1^+ < \dots$ such that $\tau_k^\pm \to \infty$ as $k \to \infty$ and for large k, the altitude $h(t), t \in [\tau_k^-, \tau_k^+]$ runs over the entire $[h_-, h_+]$ with the constant vertical velocity $\dot{h} \equiv \pm v_h$, where the sign reverses as k increases by one.

Since $d(t) \to d_0$ and the robot travels over a connected path, the robot is, as a rule, constantly close to a certain connected component C of S_t^e since some time. If $v_h \approx 0$, its motion with the speed $v \gg v_h$ looks like spiralling around C, whereas the requirement of running the entire range $[h_-, h_+]$ needs and anticipates the assumption that C spans from h_- to h_+. For steady fields, the robot sweeps the whole of C with an error proportional to v_h as t runs over $[\tau_k^-, \tau_k^+], k \approx \infty$ by [21, Lemma 4.1] and so an arbitrarily high density of coverage can be achieved by picking v_h small enough.

We use the classic model of the 3D unicycle [18]:

$$\dot{\boldsymbol{r}} = v\boldsymbol{\imath}, \quad d\boldsymbol{\imath}/dt = \boldsymbol{u} \in \mathbb{R}^3, \quad \langle \boldsymbol{u}; \boldsymbol{\imath} \rangle = 0, \quad \|\boldsymbol{u}\| \le \overline{u}, \quad (1)$$

where $\overline{u} > 0$ is given and $\boldsymbol{u}$ is the control input. The equation $\|\boldsymbol{\imath}\| \equiv 1$ from the definition of $\boldsymbol{\imath}$ is maintained true thanks to $\langle \boldsymbol{u}; \boldsymbol{\imath} \rangle = 0$ from (1) and in turn means that the robot's speed is constantly v. By (1), the robot can follow paths whose curvature does not exceed $\overline{u}/v$. According to [18, Rem. 2.1], the model (1) applies to, e.g., fixed-wing UAV's, torpedo-like UUV's, helicopters, to name just a few examples, and in this model, the control $\boldsymbol{u}$ can be replaced by the pitch q and yaw r rates due to a one-to-one correspondence $\boldsymbol{u} \leftrightarrow (q, r)$.

III. THE PROPOSED CONTROL LAW

We introduce a control law that is well posed only if the robot is not vertically oriented: $\sin \sphericalangle(\boldsymbol{\imath}, \boldsymbol{h}) \neq 0$. Then the projection $\boldsymbol{h} - \boldsymbol{\imath} \cos \sphericalangle(\boldsymbol{\imath}, \boldsymbol{h})$ of the vertical vector $\boldsymbol{h}$ onto the plane P normal to $\boldsymbol{\imath}$ is nonzero and so its scaling $\boldsymbol{\imath}_h := \frac{\boldsymbol{h} - \boldsymbol{\imath} \cos \sphericalangle(\boldsymbol{\imath}, \boldsymbol{h})}{\sin \sphericalangle(\boldsymbol{\imath}, \boldsymbol{h})}$ to the unit length is well defined.

We propose a switching controller with three modes: $\mathfrak{P}$ (preliminary), $\mathfrak{S}^+$ (spiralling upward), and $\mathfrak{S}^-$ (spiralling downward). Two its parameters $T_p > 0$ and $v_h > 0$ have the meaning of the duration of mode $\mathfrak{P}$ and the desired vertical speed, respectively; the latter defines the *desired vertical velocity*:

$$v_\ddagger := 0 \text{ in } \mathfrak{P}, \ v_\ddagger := v_h \text{ in } \mathfrak{S}^+, \ v_\ddagger := -v_h \text{ in } \mathfrak{S}^-.$$

The controller starts in mode $\mathfrak{P}$; the switching logic is given by Fig. 1. The control input is generated as follows:

$$\begin{aligned} \boldsymbol{u} = & -\overline{u}_h \cdot \mathbf{sgn}\left[\dot{h} - v_\ddagger\right] \boldsymbol{\imath}_h \\ & + \overline{u}_d \cdot \mathbf{sgn}\left[\dot{d} + \chi(d - d_0)\right] \boldsymbol{\imath}_h \times \boldsymbol{\imath}. \quad (2) \end{aligned}$$

Here $\overline{u}_d \in (0, \overline{u})$ and the map $\chi(\cdot)$ are selectable and tunable, and

$$\overline{u}_h := \sqrt{\overline{u}^2 - \overline{u}_d^2}. \quad (3)$$

Since $\boldsymbol{\imath}_h, \boldsymbol{\imath}_h \times \boldsymbol{\imath}, \boldsymbol{\imath}$ are all unit vectors and they are perpendicular to one another, the third and fourth relations from (1) are satisfied for $\boldsymbol{u}$ given by (2), as is required. Since the proposed controller is discontinuous, the solutions of the closed-loop system are meant in the sense of Filippov's definition [22]. Any method that gives access to the time derivatives $\dot{h}, \dot{d}$ is welcome; numerical differentiation is among them.

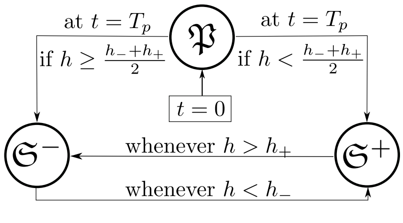

Fig. 1. Switching logic

IV. NECESSARY CONDITIONS FOR THE MISSION TO BE FEASIBLE AND ASSUMPTIONS OF THEORETICAL ANALYSIS

We first disclose requirements that are necessary for the mission to be feasible. To this end, we define the *horizontal section* (of the isosurface) at the altitude h_* as the dynamic curve given by $C_t(d_0|h_*) := \{\boldsymbol{r} \in S_t(d_0) : h(\boldsymbol{r}) = h_*\}$. For any time t_* and point $\boldsymbol{r}_*$, the dynamic isosurface $S_t(d_*), d_* := D(\boldsymbol{r}_*, t_*)$ and horizontal section $C_t(d_*|h_*), h_* := h(\boldsymbol{r}_*)$ that pass through $\boldsymbol{r}_*$ at time t_* are said to be *associated*. We also need the following notations:

- ∇D, spatial gradient of the field;
- $N(t, \boldsymbol{r}) = \nabla D(t, \boldsymbol{r}) / \|\nabla D(t, \boldsymbol{r})\|$, unit vector normal to the associated isosurface;
- $\alpha_h = \arcsin \langle N; \boldsymbol{h} \rangle$, angle between N and the horizontal;
- $N_{\boldsymbol{h}}^{\dashv} = (N - \boldsymbol{h} \sin \alpha_h) / \cos \alpha_h$, normalized projection of N onto the horizontal plane;
- $\boldsymbol{h}_N^{\dashv} = (\boldsymbol{h} - N \sin \alpha_h) / \cos \alpha_h$, normalized projection of $\boldsymbol{h}$ onto the plane tangential to the isosurface;

- $\vec{\tau} = \boldsymbol{h} \times N / \cos \alpha_h$, unit vector tangential to the associated horizontal section;
- D'', spatial Hessian;
- $\mathbf{II}[V;V] = -\langle D''V;V\rangle / \|\nabla D\|$, second fundamental form (shape tensor) of the associated isosurface;
- $\lambda(t, \boldsymbol{r})$, velocity of the isosurface in the front direction;
- $\alpha(t, \boldsymbol{r})$, acceleration of the isosurface in the front direction;
- $\vec{\omega}(t, \boldsymbol{r})$, angular velocity at which the isosurface with the fixed field value rotates with respect to itself;
- $\rho(t, \boldsymbol{r})$, density of isosurfaces;[1]
- $g_\rho(t, \boldsymbol{r})$, proportional growth rate of ρ with time;
- $\mathbb{V}\rho(t, \boldsymbol{r})$, tangential proportional gradient of the density, i.e., the tangential (to the associated isosurface) vector such that for any tangential vector V,

$$\langle \mathbb{V}\rho; V\rangle = \frac{1}{\rho(t, \boldsymbol{r})} \lim_{\Delta s \to 0} \frac{\rho(t, \boldsymbol{r} + V\Delta s) - \rho(t, \boldsymbol{r})}{\Delta s}.$$

- $n_\rho(t, \boldsymbol{r})$, normal proportional growth rate of ρ:

$$n_\rho(t, \boldsymbol{r}) := \frac{1}{\rho(t, \boldsymbol{r})} \lim_{\Delta s \to 0} \frac{\rho(t, \boldsymbol{r} + N\Delta s) - \rho(t, \boldsymbol{r})}{\Delta s}.$$

Rigorous definitions of these quantities and their expressions in terms of the field derivatives can be found in [14], [23] for 2D setting; extension of these on fields in 3D is straightforward.

Now we unveil conditions necessary for the mission to be feasible with vertical speeds $v_h \approx 0$, more precisely, with $v_h \to 0$. This focus is justified just after Definition 1.

Proposition 1: Suppose that the robot can trace the horizontal section $C_t(d_0|h_*)$ at any altitude $h_* \in [h_-, h_+]$, starting at any time in any tangential direction from any location on this section. Suppose also that in a vicinity of this section, the field $D(\cdot)$ has continuous first and second derivatives, and $\nabla D(\cdot, \cdot) \neq 0$. Then at any time and at any point of S_t^e,

$$|\lambda| \leq v \cos \alpha_h. \tag{4}$$

If additionally N is not vertical (i.e., $\cos \alpha_h \neq 0$), then

$$\overline{u}\sqrt{v^2 \cos^2 \alpha_h - \lambda^2} \geq \Big|\mathbf{II}[V_\pm; V_\pm] + \alpha + 2\,\langle \vec{\omega}; V_\pm\rangle \Big|, \tag{5}$$

$$\text{where } V_\pm := \lambda \tan \alpha_h \boldsymbol{h}_N^{\dashv} \pm \vec{\tau}\sqrt{v^2 - \lambda^2 \cos^{-2} \alpha_h}$$

and the inequality holds with any sign in ±.

To drive the output d to the targeted value, some form of output controllability is commonly needed. So the given value of d should not predetermine the sign of $\dot{d}$ and, moreover, when moving over an isosurface $\dot{d} = 0$, the robot should be free to get off it with making the field value both larger and smaller, i.e., any sign of the second time-derivative $\ddot{d}$ can be set by choosing a proper feasible control $\boldsymbol{u}$. It can be demonstrated that controllability in this sense is equivalent to (4), (5) with $\leq$ being replaced by $<$.[2]

We assume that the robot is controllable in this sense irrespective of its position within the zone of operation $\mathcal{M}$. For the sake of convenience, $\mathcal{M}$ is delineated in terms of the extreme values $h_- < h_+$ and $d_- < d_+$ ($d_0 \in [d_-, d_+]$) taken in this zone by h and d, respectively. We also take into account that when reaching the extreme altitudes $h_\pm$ with the speed $v_h > 0$, the robot cannot instantly reverse the vertical velocity and so transitions between coiling upwards and downwards involve violation of $h \in [h_-, h_+]$. So we choose an admissible extent $\Delta_h > 0$ of violation and put

$$\mathcal{M} := \{(t, \boldsymbol{r}) : d_- \leq D \leq d_+, \pm(h - h_\pm) \leq \Delta_h\}. \tag{6}$$

We also take precautions against degeneration of the afore-discussed strict inequalities into equalities, provided that time or location $\boldsymbol{r}$ go to infinity. Finally, we arrive at the following.

Assumption 1: The field $D(\cdot, \cdot)$ is twice continuously differentiable in a vicinity of the domain (6) and its horizontal section at any altitude from $[h_-, h_+]$ is not empty. There are constants $\Delta_u > 0$ and $\Delta_\lambda > 0$ such that the following enhancements of (4) and (5) hold everywhere in the zone $\mathcal{M}$:

$$|\lambda| \leq v \cos \alpha_h - \Delta_\lambda, \tag{7}$$

$$\begin{aligned} &\overline{u}\sqrt{v^2 \cos^2 \alpha_h - \lambda^2} \\ &\geq \Big|\mathbf{II}[V_\pm; V_\pm] + \alpha + 2\,\langle \vec{\omega}; V_\pm\rangle \Big| + \Delta_u. \end{aligned} \tag{8}$$

Since the smooth trajectory of the robot should lie on the isosurface, it is natural to exclude singularities of the isosurface.

Assumption 2: In the domain (6), the field has no spatial singularities $\nabla D \neq 0$, and this trait does not degenerate: there is a constant $b_\rho > 0$ such that $\|\nabla D(t, \boldsymbol{r})\| \geq b_\rho^{-1}\ \forall (t, \boldsymbol{r}) \in \mathcal{M}$.

Assumption 3: The quantities $g_\rho, n_\rho, \mathbb{V}\rho, \lambda, \vec{\omega}, \varkappa$ are bounded in the operational zone:

$$\begin{aligned} |g_\rho| \leq b_g, \quad |n_\rho| \leq b_n, \quad \|\mathbb{V}\rho\| \leq b_\nabla, \quad |\lambda| \leq b_\lambda, \\ \|\vec{\omega}\| \leq b_\omega, \quad \varkappa \leq b_\varkappa \qquad \forall (t, \boldsymbol{r}) \in \mathcal{M}, \end{aligned} \tag{9}$$

where $\varkappa$ is the maximal (unsigned) principal curvature of the associated isosurface (equivalently, the maximal in absolute value eigenvalue of the second fundamental form $\mathbf{II}$) and the constants $b_g, b_n, b_\nabla, b_\lambda, b_\omega, b_\varkappa$ do not depend on $(t, \boldsymbol{r}) \in \mathcal{M}$.

Before the proposed control law is put in use, the robot is set in a special posture. We omit discussion of possible transient maneuvers because of their banality and merely state their desired outcome as the following.

Assumption 4: The initial position of the robot $(\boldsymbol{r}_{\text{in}}, \boldsymbol{\imath}_{\text{in}})$ is with $h \in (h_-, h_+)$ and a horizontal orientation $\langle \boldsymbol{\imath}_{\text{in}}; \boldsymbol{h}\rangle = 0$.

Under this assumption, choosing the continuous control input so that $\langle \vec{u}; \boldsymbol{h}\rangle \equiv 0$ and

$$\|\vec{u}\| \equiv \overline{u} \tag{10}$$

ensures that the robot makes either left or right turn in the initial horizontal plane. In any case, $2\pi/\overline{u}$ units of time are need to perform the full turn and the respective path is a circle. The disc $\mathcal{D}_{\text{in}}^{l/r}$ bounded by this circle is said to be *initial*, where the index l or r is used in the case of the left and right turn, respectively. We finally require that both $\mathfrak{D}^{l}_{\text{in}}$ and $\mathfrak{D}^{r}_{\text{in}}$ are covered by the zone (6), and the turning rate of the robot exceeds the average rate of rotation of the isosurface associated with the initial location $\boldsymbol{r}_{\text{in}}$ about the vertical axis, where averaging is over some initial time interval.

---

[1] It evaluates how many isosurfaces lie within the unit distance from $S(d_*)$, where their "number" is assessed by the range of the associated field values.

[2] After this replacement, (4) implies that $\cos \alpha_h \neq 0$.

Assumption 5: There exists a natural number k such that during the interval $[0, T_k]\,, T_k := 2\pi k/\overline{u}$ **(i)** the projection $N^{\dashv}_{\boldsymbol{h}}(t, \boldsymbol{r}_{\text{in}})$ of the unit normal onto the horizontal plane rotates by less than $2\pi(k-1)$ and **(ii)** the zone (6) contains the initial discs: $d_- < D(t, \boldsymbol{r}) < d_+ \; \forall t \in [0, T_k], \boldsymbol{r} \in \mathfrak{D}^{l/r}_{\text{in}}$.

V. MAIN RESULTS

Our first result shows that the controller from Sect. III is inherently capable to execute the mission under the assumptions, which are inevitable to some extent, as is advocated in Sect. IV.

Theorem 1: Suppose that Assumptions 1–5 hold. Then the parameters $v_h, \overline{u}_h, \overline{u}_d, \chi(\cdot), T_p$ of the control law from Section III can be chosen so that the closed-loop system presents the following properties:

(i) The robot performs coiling sweep coverage of the isosurface, as detailed in Definition 1;

(ii) The robot is never oriented vertically $\boldsymbol{\imath} \times \boldsymbol{h} \neq 0 \; \forall t$.

Moreover, let $Q_{\text{in}} = \{(\boldsymbol{r}, \boldsymbol{\imath})\}$ be a compact set of initial states that satisfy Assumptions 4 and 5 (with a common k). For any $\overline{v}_h > 0$, common values of the above parameters can be chosen so that the claims (i) and (ii) are true with the speed of the vertical drift $v_h \leq \overline{v}_h$ whenever the initial state belongs to Q_{in}.

Now we turn to specific recommendations on controller tuning. Two parameters $\overline{u}_d, \chi(\cdot)$ are chosen in two steps: the bounds given at the first step are enhanced at the second one.

Preliminary choice of $\overline{u}_d$ from (2). Putting $\overline{u} := \overline{u}_d$ in (10) gives rise to larger disks $\mathfrak{D}^{l/r}_{\text{in}}(\overline{u}_d) \supset \mathfrak{D}^{l/r}_{\text{in}}$. For $\overline{u}_d \approx \overline{u}$, they are close to $\mathfrak{D}^{l/r}_{\text{in}}$ and so lie inside the zone (6) for $t \in [0, T_k]$ due to Assumption 5. Hence, Assumption 5 remains true after replacing $\overline{u}$ by $\overline{u}_d$ if $\overline{u}_d < \overline{u}$ is close enough to $\overline{u}$. (This is true uniformly over all initial states from Q_{in} in the context of the last claim from Theorem 1.) Such $\overline{u}_d \in (0, \overline{u})$ is chosen; it may be increased at a subsequent step of tuning.

Preliminary choice of $\chi(\cdot)$ from (2): This is a continuous and piece-wise smooth function such that

$$\chi(0) = 0, \quad \chi(z) > 0 \; \forall z > 0, \quad \chi(z) < 0 \; \forall z < 0, \tag{11}$$

$$\overline{\chi} := \sup_{z \in \mathbb{R}} |\chi(z)| < \infty, \quad \overline{\chi}' := \sup_{z \in \mathbb{R}} |\chi'(z\pm)| < \infty, \tag{12}$$

$$\chi_\rho := b_\rho \overline{\chi} < \Delta_\lambda,$$

where b_ρ is taken from Assumption 2. Relations (11) and (12) are met by, e.g., the linear function with saturation and by $\chi(z) = a \arctan(z/b), a, b > 0$. The upper bounds $\overline{\chi}, \overline{\chi}'$ from (12) may be enhanced at the next step.

Final choice of $\overline{u}_d, \chi(\cdot), v_h$. To serve it, a real $\eta \in (0, 1)$ is picked and the parameters are subjected to the following:

$$(v_{h,\chi} + 2b_\lambda) v_{h,\chi} < (1 - \eta^2) \Delta_\lambda^2, \quad v_{h,\chi} := v_h + \chi_\rho; \tag{13}$$

$$\begin{aligned} & v\sqrt{\overline{u}^2 - \overline{u}_d^2} + \chi_\rho(\chi_\rho b_n + 2v b_\nabla + 2b_g) \\ & + [2v b_\varkappa + b_\omega] \, v \frac{\sqrt{(v_{h,\chi} + 2b_\lambda)^2 + 4\eta^2 \Delta_\lambda^2}}{\eta \Delta_\lambda^2} v_{h,\chi} \\ & + \frac{\overline{u}(v_{h,\chi} + 2b_\lambda) v_{h,\chi}}{2\eta \Delta_\lambda} + v|\overline{u} - \overline{u}_d| + \overline{\chi}\overline{\chi'} < \Delta_u, \end{aligned} \tag{14}$$

$$v_h < \min\{v, \overline{v}_h\}, \; v - \sqrt{v^2 - v_h^2} < \Delta_h \sqrt{\overline{u}^2 - \overline{u}_d^2}. \tag{15}$$

Here $v, \overline{u}$ are taken from (1), Δ_λ, Δ_u from (7), (8), $b_\lambda, b_n, b_\nabla, b_g, b_\varkappa, b_\omega$ from (9), and $\overline{v}_h$ from Theorem 1. Relations (13)—(15) are feasible. Indeed, since the l.h.s. of both (13) and (14) goes to 0 as $v_h \to 0, \overline{\chi} \to 0, \overline{\chi}' \to 0, \overline{u}_d \to \overline{u}$, whereas the r.h.s. is a positive constant, (13) and (14) are satisfied by all small enough $v_h, \overline{\chi}, \overline{\chi}'$ and $\overline{u}_d$ close enough to $\overline{u}$. This is used to put extra bounds on $\chi(\cdot)$ in (12) and $\overline{u}_d$, after which the final choice of $\chi(\cdot)$ and $\overline{u}_d$ is performed. Then (15) can be met by further decreasing v_h, if necessary.

Parameter $\overline{u}_h$ from (2) is defined by (3).

T_p from Fig. 1: $T_p \geq 2\pi k/\overline{u}_d$, where k is taken from Assumption 5.

Theorem 2: Let Assumptions 1–5 be true. Suppose that the parameters of the navigation law meet the above recommendations. Then the claims (i) and (ii) of Theorem 1 are valid for all initial states from Q_{in}.

VI. COMPUTER SIMULATION TESTS

Table I lists the numerical values of the basic parameters used in the simulations; the symbol ❡ stands for the unit of measurement of the field value. Control update period was 0.1 s, and the readings of d and h were contaminated by Gaussian additive noises with standard deviation $\sigma = 0.1$ m in all cases. A linear function with saturation was chosen as $\chi(\cdot)$:

$$\chi(p) := \begin{cases} \mu p/\delta & \text{if } |p| \leq \delta \\ \operatorname{sgn}(p)\mu & \text{otherwise} \end{cases}$$

where $\delta = 5$ ❡ and $\mu = 0.4$ ❡/s. Simulations were performed using MATLAB. Multimedia of the extended versions of all test are available at `goo.gl/ankgVA`.

TABLE I
PARAMETERS USED FOR SIMULATION

$d_0 = 10$ ❡	$v = 10$ m/s	$v_h = 0.05$ m/s
$T_p = 15$ s	$\bar{u} = 5$ rad/s	$\bar{u}_h = 0.05$ rad/s

The first test deals with the fairly simple scenario of a radial and steady scalar field $D(\boldsymbol{r}) = f(\|\boldsymbol{r} - \boldsymbol{r}_0\|)$, where $\boldsymbol{r}_0$ is its center and the smooth function $f(d)$ increases from 0 without limits as $d \geq 0$ grows up. Its isosurfaces are spheres, whose totality is depicted in Fig. 2(a–b). The targeted d_0-isosurface is the sphere with a radius of 50 m. Starting from a remote location, the robot quickly reaches the desired d_0-isosurface, as is shown in Fig. 2(a). Then it starts moving over this isosurface, while coiling around it upwards; a principal part of this maneuver is shown in Fig. 2(b). After reaching the upper end of the altitudinal range $h_+ = 135$ m, the robot proceeds with moving over the isosurface, while coiling downwards. This maneuver is terminated on reaching the lower end $h_- = 65$ m of the assigned altitudinal range. After this an upward coiling is commenced, and so on. Fig. 2(c) displays an excellent performance of the algorithm during six cycles of upward/downward coiling, despite of the measurement errors.

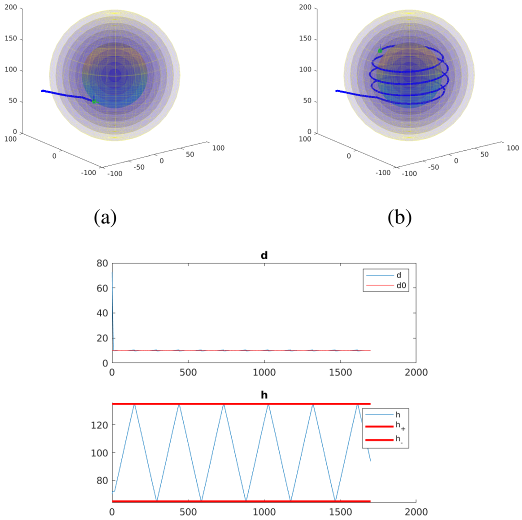

(a) (b)

(c)

Fig. 2. Tracking a steady spherical isosurface

The next scenarios are more challenging: they deal with unsteady fields and isosurfaces with rather sophisticated shapes. This troubles visualization of the results in 3D so that we depict only one surface that consists of points at a given (small) distance from the targeted isosurface and inherits its shape.[3]

In Fig. 3, the targeted isosurface looks like a vertical 3D five pointed star circumvented by circle of 140 m diameter. The star moves along a circular orbit with a radius of 50 m with the angular velocity ≈ 0.1 rad/s. While monitoring the altitudinal range between $h_- = 50$ m and $h_+ = 155$ m, the robot faces the situations where the horizontal section of the surface splits into several connected components, as is illustrated in Fig. 3(d) (which details Fig. 3(c)), and so the robot has to choose which of the related 3D "rays" of the star should be swept over. As follows from Fig. 3(e), the algorithm makes the "right" choice by picking the only ray that rises up to h_+, while having other options open to it. In this (and the next) test, the necessary condition (5) is violated: near the points where the "rays" meet each other, the second fundamental form $\mathbf{II}[\cdot;\cdot]$ is excessively large. (We recall that this form is responsible for the curvatures of the normal sections of the surface.) Although arrival at exactly such a point does not seem as highly probable, this does happen in the test and causes an acute splash of d at $t \approx 150$ s in Fig. 3(e). Overall, the robot quickly reaches the desired d_0-isosurface and then effectively monitors it, in spite of the surface motion and violation of the necessary conditions.

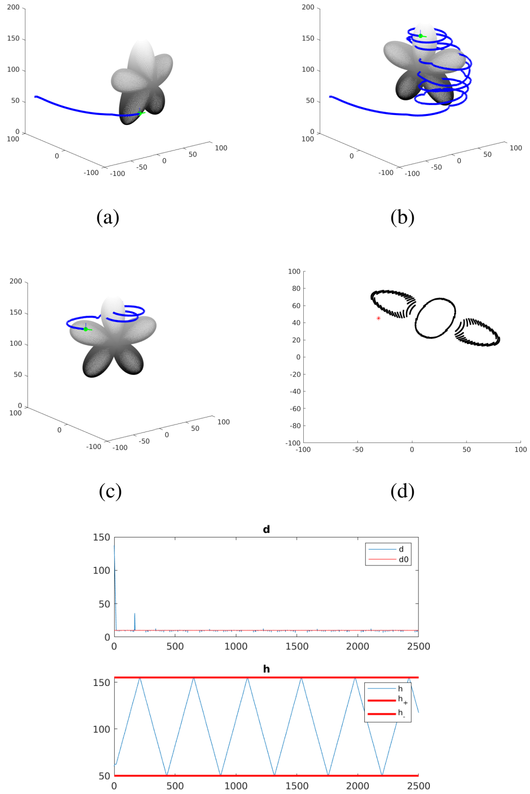

(a) (b)

(c) (d)

(e)

Fig. 3. Tracking a boundary moving along the orbit

Fig. 4 is concerned with a field whose isosurface has a rather irregular shape: it not only combines convexities with concavities but also has three non-identical protrusions, each glued to the bottom of the surface main body and in the form of an irregularly deformed bubble. The field slowly rotates about a vertical axis.[4] Violation of condition (5)[5] is more systematic: it holds not only at the junction of the bubbles but also at the bottom of the vertical coombs (see Fig. 4(a)) and at the top of the vertical ridges (see Fig. 4(c)). Unlike the junctions, the robot has to regularly cross these tops and bottoms when coiling around the surface. So in Fig. 4(g) the vertical splashes do not look like a one-time occurrence; howbeit, the eventual average field error is ≈ 1.3 ¶, which looks as a good outcome in face of the surface intricacies. As is highlighted in Fig. 4(f), lower horizontal sections of the surface split into three connected components; every of them is attributed to a particular “bubble” and spreads down to the lower end ≈ 50 m of the patrolled altitudinal range. In different rounds of coiling around the surface, the algorithm chooses different “bubbles” to be swept. In Fig. 4(e), the small compact coil is the result of coiling around the tightest “bubble”; the snapshot corresponds to a moment when this “bubble” has moved to the invisible background. Overall, the robot still satisfactory solves the mission, although the convergence in Fig. 4(g) is not as regular as in Figs. 2, 3.

---

[3] We prefer this surface to resolve the dilemma between drawing S as non-transparent or transparent: in the first case, robot's path looks dashed and incomplete due to vanishing from view of its parts that are not only behind S but also inside S; in the second case, the picture becomes oversaturated with details, the path looks as highly entangled and is poorly comprehensible.

[4] Because of the motion of the surface, the past path of the robot looks as if penetrating the surface in some snapshots. In fact, the path bypasses the surface, as can be seen from the multimedia at `goo.gl/ankgVA`.

[5] We recall that in particular, it subdues the surface contortion to the turning capacity of the robot.

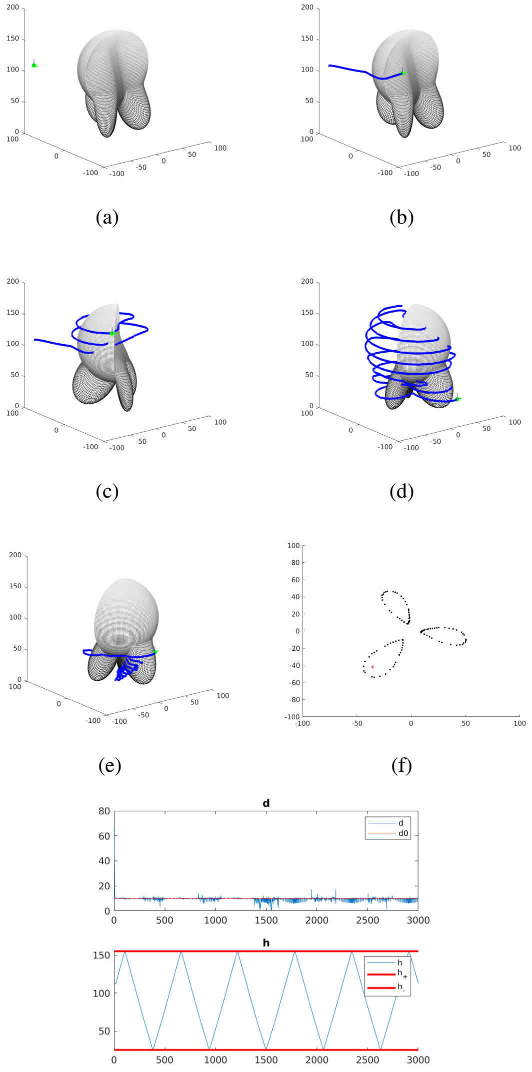

(a) (b)

(c) (d)

(e) (f)

(g)

Fig. 4. Tracking a rotating sophisticated boundary

REFERENCES

[1] B. A. White, A. Tsourdos, I. Ashokoraj, S. Subchan, and R. Zbikowski, “Contaminant cloud boundary monitoring using UAV sensor swarms,” in *Proceedings of the AIAA Guidance, Navigation, and Control Conference*, San Francisco, CA, August 2005.

[2] L. Pettersson, D. Durand, O. Johannessen, and D. Pozdnyakov, *Monitoring of Harmful Algal Blooms*. UK: Praxis Publishing, 2012.

[3] D. Marthaler and A. L. Bertozzi, “Tracking environmental level sets with autonomous vehicles,” in *Recent Developments in Cooperative Control and Optimization*, S. Butenko, R. Murphey, and P. Pardalos, Eds. Boston: Kluwer Academic Publishers, 2003, vol. 3.

[4] A. Bertozzi, M. Kemp, and D. Marthaler, “Determining environmental boundaries: Asynchronous communication and physical scales,” in *Cooperative Control*, V. Kumar, N. Leonard, and A. Morse, Eds. Berlin: Springer Verlag, 2004, pp. 25 – 42.

[5] S. Srinivasan, K. Ramamritham, and P. Kulkarni, “ACE in the hole: Adaptive contour estimation using collaborating mobile sensors,” in *Proc. of the Int. Conference on Information Processing in Sensor Networks*, April 2008, pp. 147 – 158.

[6] M. H. S. Loizou and V. Kumar, “Stabilization of multiple robots on stable orbits via local sensing,” in *Proc. of the IEEE Conference on Robotics and Automation*, April 2007, pp. 2312 – 2317.

[7] F. Zhang and N. E. Leonard, “Cooperative control and filtering for cooperative exploration,” *IEEE Transactions on Automatic Control*, vol. 55, no. 3, pp. 650–663, 2010.

[8] J. Zhipu and A. Bertozzi, “Environmental boundary tracking and estimation using multiple autonomous vehicles,” in *Proceedings of the 46th IEEE Conference on Decision and Control*, New Orleans, Lu, December 2007, pp. 4918–4923.

[9] A. Joshi, T. Ashley, Y. Huang, and A. Bertozzi, “Experimental validation of cooperative environmental boundary tracking with on-board sensors,” in *Proc. of the American Control Conference*, June 2009, pp. 2630 – 2635.

[10] C. Barat and M. Rendas, “Benthic boundary tracking using a profiler sonar,” in *Proc. of the IEEE/RSJ International Conference on Intelligent Robots and Systems*, October 2003, pp. 830 – 835.

[11] D. Casbeer, S. Li, R. Beard, T. McLain, and R. Mehra, “Forest fire monitoring using multiple small UAVs,” *Proc. of the 2005 American Control Conference*, vol. 5, pp. 3530–3535, June 2005.

[12] D. Baronov and J. Baillieul, “Reactve exploration through following isolines in a potential field,” in *in Proceedings of the American Control Conference*, NY, December 2007, pp. 2141–2146.

[13] A. Matveev, H. Teimoori, and A. Savkin, “Method for tracking of environmental level sets by a unicycle-like vehicle,” *Automatica*, vol. 48, no. 9, pp. 2252–2261, 2012.

[14] A. Matveev, M. Hoy, K. Ovchinnikov, A. Anisimov, and A. Savkin, “Robot navigation for monitoring unsteady environmental boundaries without field gradient estimation,” *Automatica*, vol. 62, pp. 227–235, 2015.

[15] M. Owen, R. Beard, and T. McLain, “Implementing Dubins airplane paths on fixed-wing UAVs,” in *Handbook of Unmanned Aerial Vehicles*, K. Valavanis and G. Vachtsevanos, Eds. Dordrecht: Springer, 2015, pp. 1677–1701.

[16] H. Marino, P. Salarisz, and L. Pallottino, “Controllability analysis of a pair of 3D Dubins vehicles in formation,” *Robotics and Autonomous Systems*, vol. 83, pp. 94–105, 2016.

[17] A. Matveev, H. Teimoori, and A. Savkin, “Navigation of a unicycle-like mobile robot for environmental extremum seeking,” *Automatica*, vol. 47, no. 1, pp. 85–91, 2011.

[18] A. Matveev, M. Hoy, and A. Savkin, “3D environmental extremum seeking navigation of a nonholonomic mobile robot,” *Automatica*, vol. 50, no. 7, pp. 1802–1815, 2014.

[19] A. Matveev, A. Semakova, and A. Savkin, “Range-only based circumnavigation of a group of moving targets by a non-holonomic mobile robot,” *Automatica*, vol. 65, pp. 76–89, 2016.

[20] ——, “Tight circumnavigation of multiple moving targets based on a new method of tracking environmental boundaries,” *Automatica*, vol. 79, pp. 52–60, 2017.

[21] A. Matveev, K. Ovchinnikov, and A. Savkin, “Proofs of the technical results justifying an algorithm of reactive 3D navigation for a surface scan by a nonholonomic mobile robot,” 2016, online; `http://arxiv.org/abs/1605.02577` .

[22] A. Filippov, *Differential Equations with Discontinuous Righthand Sides*. Dordrecht, the Netherlands: Kluwer, 1988.

[23] A. Matveev, M. Hoy, and A. Savkin, “Proofs of the technical results justifying an algorithm of extremum seeking navigation in dynamic environmental fields,” 2015, online; `http://arxiv.org/abs/1502.02224` .